Quaternary Science Reviews 29 (2010) 8–20

Contents lists available at ScienceDirect

Quaternary Science Reviews

journal homepage: www.elsevier.com/locate/quascirev

Consistent dating for Antarctic and Greenland ice cores

Bénédicte Lemieux-Dudon [a,*], Eric Blayo [b], Jean-Robert Petit [a], Claire Waelbroeck [c], Anders Svensson [d], Catherine Ritz [a], Jean-Marc Barnola [a], Bianca Maria Narcisi [e], Frédéric Parrenin [a]

[a] CNRS/Université Joseph Fourier, Grenoble 1, LGGE 38402, St Martin d'Hères cedex, France
[b] LJK, BP 53, F-38041 Grenoble Cedex, France
[c] LSCE/IPSL, Laboratoire CNRS-CEA-UVSQ, Domaine du CNRS, 91198 Gif-sur-Yvette, France
[d] Ice and Climate Group, Niels Bohr Institute, Copenhagen, Denmark
[e] ENEA Rome, Italy

ARTICLE INFO

Article history:
Received 10 February 2009
Received in revised form
6 November 2009
Accepted 9 November 2009

ABSTRACT

We are hereby presenting a new dating method based on inverse techniques, which aims at calculating consistent gas and ice chronologies for several ice cores. The proposed method yields new dating scenarios simultaneously for several cores by making a compromise between the chronological information brought by glaciological modeling (i.e., ice flow model, firn densification model, accumulation rate model), and by gas and ice stratigraphic constraints. This method enables us to gather widespread chronological information and to use regional or global markers (i.e., methane, volcanic sulfate, Beryllium-10, tephra layers, etc.) to link the core chronologies stratigraphically. Confidence intervals of the new dating scenarios can be calculated thanks to the probabilistic formulation of the new method, which takes into account both modeling and data uncertainties. We apply this method simultaneously to one Greenland (NGRIP) and three Antarctic (EPICA Dome C, EPICA Dronning Maud Land, and Vostok) ices cores, and refine existent chronologies. Our results show that consistent ice and gas chronologies can be derived for depth intervals that are well-constrained by relevant glaciological data. In particular, we propose new and consistent dating of the last deglaciation for Greenland and Antarctic ice and gas records.

1. Introduction

The reconstruction of past climates is a critical step to understand future climate changes. Fortunately, past climatic events were recorded in numerous paleo-archives: trees, speleothems, terrestrial cores, marine cores and ice cores. A consistent dating of paleo-archives (i.e., a dating that enables us to compare the timing and the duration of events recorded in the different archives) is a prerequisite for the construction and interpretation of climatic scenarios. This issue remains a complex one, and we here focus on deep ice cores and the consistency of their dating.

One specific issue related to ice core dating is the age difference (hereafter delta-age) between the trapped gas and the surrounding ice matrix: gas is trapped several tens of meters below the ice-sheet surface, where it is surrounded by ice that was deposited as surface snow, hundreds or thousands of years earlier. This feature causes a two-fold dating puzzle: for each drilling, the dating of both the gas and ice records must be assessed.

Numerous strategies are currently applied for dating the ice matrix and the gas phase along ice cores: (i) wiggle matching of ice core records to insolation time series (i.e., orbital tuning), (ii) wiggle matching of ice core records to other dated paleo-archives (ice, marine or terrestrial cores…), (iii) identification of dated volcanic horizons (e.g., tephra layers, sulfate spikes for the last millennium), (iv) counting of annual layers and (v) ice flow modeling for dating the ice, combined with firn densification modeling to estimate the delta-age.

Some dating strategies only provide a single temporal constraint (e.g., tephra layers) while others help to constrain the entire core (e.g., ice flow modeling or orbital tuning). The accuracy of a dating constraint may decrease with depth (as is the case for annual layer counting and ice flow modeling), or remain rather steady but be poor or questionable (e.g., orbital tuning, matched paleo-events with a poor understanding of their link through the climatic system).

One special feature of glaciological models is a large model error due to unresolved physics and errors on the forcing fields, clearly

* Corresponding author.
E-mail address: benedicte.lemieux@imag.fr (B. Lemieux-Dudon).

0277-3791/$ – see front matter
doi:10.1016/j.quascirev.2009.11.010

affecting the quality of the inferred dating scenarios[1]. Inverse modeling is therefore particularly relevant for the improvement of ice core dating. Parrenin et al. (2001) and Grinsted and Dahl-Jensen (2002) applied inverse modeling techniques to simple ice flow models in order to constrain several poorly-known parameters (i.e., glacial-interglacial change in accumulation rate, prescribed velocity profiles, basal sliding and melting, etc.). Such methods have been used to construct age models for East Antarctic and Greenland ice cores (EPICA Community Members, 2004; Parrenin et al., 2004, 2007b).

The dating of a single ice core involves extensive work (e.g., measurements, modeling and synthesis). For that reason, one strategy consists of obtaining a reference chronology for a given ice core, which is then wiggle matched to several other cores (Ruth et al., 2007; Rasmussen et al., 2008). Common paleo-events that are recorded on two or more ice cores enable the wiggle matching. Such common events are referred to as "regional or global stratigraphic markers". For the ice matrix, one can mention tephra layers (Basile et al., 2001; Narcisi et al., 2005, 2006) or volcanic sulfate spikes (Traufetter et al., 2004; Udisti et al., 2004; Severi et al., 2007; Rasmussen et al., 2008). For the gas phase, one can mention methane (EPICA Community Members (2006)) and oxygen-18 isotopic ratio of O_2 (hereafter designated with the delta notation $\delta^{18}O_{atm}$, see Capron et al., this issue, Landais et al. (2006b)).

Recently, two reference chronologies have become available for Greenland and Antarctic ice cores, respectively: (i) the GICC05 chronology built in the framework of the Greenland Ice Core Chronology 2005 initiative (hereafter GICC05 chronology) and (ii) the EDC3 chronology built for the EPICA Dome C core (hereafter EDC). GICC05 is a layer counted age scale, unified for the DYE-3, GRIP and NGRIP cores (Andersen et al., 2006; Rasmussen et al., 2006; Svensson et al., 2006, 2008), which currently extends back to 60 kyr b2 k (i.e., 1000 years before the year 2000 AD). Conversely, EDC3 is partly built with an inverse 1D flow model (Parrenin et al., 2007b), but local corrections were subsequently applied to the modeled chronology (referred to as EDC3model), in order to solve discrepancies with a number of stratigraphic markers (Parrenin et al., 2007a). Several Antarctic ice core chronologies have further been matched to EDC3. In particular, EDC3 was transferred on the EPICA Dronning Maud Land core (hereafter EDML) by the mean of volcanic markers (Severi et al., 2007), which lead to the EDML1 ice chronology (Ruth et al., 2007). Associated with ice chronologies are the gas age scales and delta-age estimates. Delta-age is usually calculated by the mean of densification models (Pimienta, 1987; Arnaud et al., 2000; Goujon et al., 2003). It is specifically associated with EDML1 and EDC3, the EDML1gas_a and EDC3gas_a gas chronologies that are also referred to as the sp4 scenario, and that are simulations made by Loulergue et al. (2007) by application of the Goujon et al. (2003) densification model. The sp4 scenario consists of a reduced glacial accumulation rate for both EDC and EDML, compared to the reference accumulation scenarios related to EDML1 and EDC3. Among several other temperature and accumulation rate scenarios tested by Loulergue et al. (2007), the sp4 scenario leads to the best agreement between the EDC and EDML methane records.

These recent studies however still raise questions. First, while methane is a global marker, the Antarctic and Greenland CH_4 records are out of phase during the last deglaciation transitions, as illustrated on the panel A in Fig. 1, where the EDC, EDML and

[1] In this text, a "glaciological model" refers to the combination of models which enable us to estimate the gas and ice chronologies of an ice core: in addition to ice flow and firn densification models, included are the models that provide the forcing fields (paleo temperature, accumulation rate and ice sheet thickness history, etc).

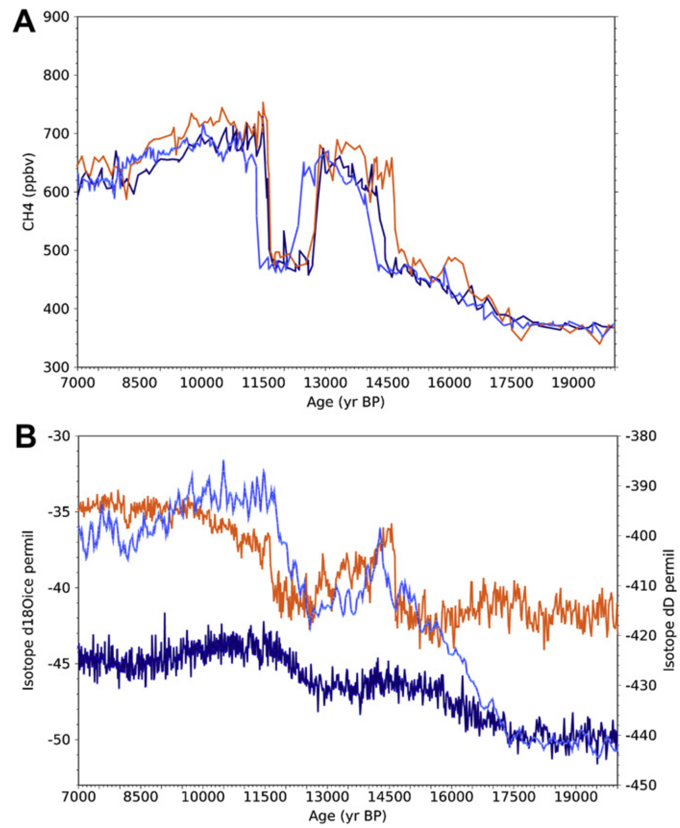

Fig. 1. Current dating problems related to ice cores of Antarctic (EDC and EDML respectively in light and dark blue) and Greenland (orange), for the last deglaciation transitions: (A) Unexpected timing during the Bolling–Allerod transition between ice isotopic records with the EDC3, EDML1 and GICC05 ice age scales, with a 400 yr lag between the maximum value reached by the EDC δD record before the Antarctic Cold Reversal, and (the fast Bolling–Allerod transition recorded in the NGRIP $\delta^{18}O_{ice}$ record, respectively for the EDC, EDML and NGRIP ice isotopes. (B) Mismatch between the CH_4 records with the sp4 gas age scenario for EDC and EDML, and the GICC05 gas age (Blunier et al., 2007) for the Greenland stack record.

Greenland methane records are plotted against the sp4 scenario and the NGRIP gas age scale (Blunier et al., 2007), respectively. Accordingly, the timing between the Antarctic and Greenland ice isotopic records is questionable during the Bolling–Allerod transition (see panel B of Fig. 1, where the records are plotted against EDC3, EDML1 and GICC05). This questionability could lead to misinterpretation of the last deglaciation triggering mechanisms, in particular whether the climate deglacial transition was initiated in the Southern or in the Northern hemisphere (Alley et al., 2002; Clark et al., 2004). Moreover, the modeling error attached to the glaciological age models is still too large: (i) the construction of EDC3, including the stratigraphy based corrections (Parrenin et al., 2007a,b), revealed that the forward ice flow models (aiming at calculating ice age scales) omit important physical mechanisms: the uncertainty attached to forward ice flow models may either be due to inaccurate forcing fields, which encompass the accumulation rate, temperature and ice sheet thickness histories, or result from inadequately described physical or mechanical processes in the ice flow, (ii) the EDC reference ice and gas chronologies (i.e., EDC3 and EDC3gas_a gas) rely on two different accumulation rate scenarios, which is inconsistent, (iii) the persistent mismatch between the EDC and EDML CH_4 records, even with the sp4 scenario, calls into question either the reconstructed accumulation rate and temperature histories (i.e., the forcing fields for the densification models), or the densification model itself. Finally, the spreading of chronological information and the complexity of chronologies have prevented the construction of robust confidence intervals, especially when the chronologies are model based.

Given the above observations, we hereby we propose a new dating method which aims at bringing solutions to the above mentioned issues. This method is a probabilistic approach based on inverse techniques. It estimates new dating scenarios by making the "best" compromise between model based dating scenarios and chronological information from data. It operates on several cores at the same, potentially covering the full depth intervals of the cores. The use of regional or global stratigraphic markers (related to the gas or ice phases) in addition to gas or ice age markers, enables us to cross-constrain the chronologies. The probabilistic formulation provides the means to estimate confidence intervals of the new dating scenario. In Section 2 we present the methodology, and in Section 3 we propose an application which involves the full ice cores of Vostok, EDC, EDML and the upper part of the NGRIP core. In Section 4 we present the overall new dating scenarios, and we focus the discussion on the 0–50 kyr time interval where the type and density of data ensure satisfying confidence. As intended, our new dating scenarios resolve the dating inconsistencies between Greenland and Antarctica, in particular during the last deglaciation.

2. Methodology

Let us suppose that we are interested in N ice cores for which we wish to simultaneously calculate and cross-constrain their age scales, and that we write χ^k for the gas and ψ^k for the ice, $\forall\ k = 1, \ldots, N$. The new dating method handles three key glaciological entities that vary along the core: (i) A^k the accumulation rate measured in meters of ice equivalent per year (hereafter m-ie/yr), (ii) T^k the total thinning function and (iii) C^k the close-off depth measured in meters of ice equivalent (hereafter m-ie). T^k is the ratio between L^k, the in situ annual layer thickness as measured today in m-ie/yr, and the initial annual layer thickness at the time of snow deposition (i.e., A^k). C^k can be deduced from the close-off depth in meters of firn material (i.e, the depth where the porous firn turns into ice and traps samples of air), by assessing D^k, the relative density profile between the core material and pure ice.

When A^k, T^k and C^k are known at any depth z^k of the core k, one can infer L^k as well as $\Delta\lambda^k$, the delta-depth. The delta-depth is the depth interval in situ that separates a past climatic event simultaneously recorded in the ice matrix and in the gas phase. In other words, $\Delta\lambda^k$ is the result of the thinning of the C^k column during its trajectory from the surface to the depth z^k:

$$L^k\left(z^k\right) = T^k\left(z^k\right)A^k\left(z^k\right) \tag{1}$$

$$\Delta\lambda^k\left(z^k\right) \approx T^k\left(z^k\right)C^k\left(z^k\right) \tag{2}$$

The two following equations show that the knowledge of A^k, T^k and C^k is sufficient to deduce χ^k and ψ^k, which are the gas and ice age scales associated with the core k, respectively (ζ^k and z^k both represent depth coordinates along the core k):

$$\psi^k\left(z^k\right) = \int_0^{z^k} \frac{D^k\left(\zeta^k\right)}{L^k\left(\zeta^k\right)} d\zeta^k \tag{3}$$

$$\chi^k\left(Z^k\right) \approx \psi^k\left(Z^k - \Delta\lambda^k\left(Z^k\right)\right) \tag{4}$$

Numerical models describing the ice flow and the firn densification can provide glaciological scenarios for A^k, T^k and C^k. Both ice flow and firn densification models rely on two empirical relationships that relate to the isotopic content of the ice, the mean annual accumulation rate as well as the mean annual temperature. Experimental evidence suggests that the forward (or inverse) glaciological models and/or the empirical relationships on which they rely are inaccurate (Landais et al., 2006a; Durand et al., 2007; Dreyfus et al., 2007; Parrenin et al., 2007a). This being understood, in this work we consider the dating scenarios based on forward or inverse glaciological models as prior or background scenarios that must be improved. For the core k, we denote the background scenario $A^{b,k}$, $T^{b,k}$, $C^{b,k}$, and the associated gas and ice chronologies $\chi^{b,k}$ and $\psi^{b,k}$.

The new dating method is a probabilistic inverse approach based on a Bayesian inference. It aims at calculating an improved dating scenario A^k, T^k, C^k for every core k involved in the dating process. The new scenario must be close to the background dating scenario, and at the same time in best agreement with the glaciological data (and especially with any conflicting evidence). For this purpose, we apply the Bayesian theorem and formulate a probabilistic compromise between the two previous constraints. To simplify the notation, we use the Y vector to describe the full set of glaciological data and we introduce X and X^b to represent the searched and the background dating scenarios (i.e., respectively A^k, T^k, C^k and $A^{k,b}$, $T^{k,b}$, $C^{k,b}$ for all the cores). The Bayesian inference measures the posterior probability $p_a(X)$ attached to any possible dating scenario X according to the prior modeling knowledge and the data constraint:

$$p_a(X) \alpha p_0(Y|X) p_b(X) \tag{5}$$

where p_b is usually called the prior or background probability density function (hereafter pdf) and p_o is the conditional pdf of measuring Y given X.

The p_b pdf describes the modeling error (i.e., the error on X^b), whereas the p_o pdf describes the "observation" error (i.e., the error on data Y). In the present work we assume that the probabilities in equation (5) are all normally distributed (or lognormally distributed, but in that case they are transformed into normal probabilities by a logarithmic change of variable). p_b therefore relates to $X - X^b$, the distance to the background dating scenario, while p_o relates to $Y - h(X)$, the distance between Y and $h(X)$, where h is the observation model and $h(X)$ predicts the data Y, X being given.

We assume that the "best" dating scenario, written X^a (i.e., $A^{a,k}$, $T^{a,k}$, $C^{a,k}$ $\forall\ k = 1, \ldots, N$), satisfies the maximum likelihood criterion, which means that $X = X^a$ maximises the posterior pdf $p_a(X)$. We derive J, the misfit function of the problem (i.e., $J = -\ln p_a$), in order to solve the inverse problem according to the maximum likelihood. The J function, which is optimised with the m1qn3 minimizer (Gilbert and Lemarechal, 1993), splits into two terms, respectively the observation term and the background term:

$$J(X) = \frac{1}{2}(Y - h(X))R^{-1}(Y - h(X))^T + \frac{1}{2}\left(X - X^b\right)B^{-1}\left(X - X^B\right)^T \tag{6}$$

where B is the background error covariance matrix and R is the observation error covariance matrix.

The B matrix accounts for the uncertainties on X^b the background dating scenario, i.e., the modeling uncertainties. The R matrix accounts for the uncertainties attached to the data used to constrain the problem. The inverse matrices, B^{-1} and R^{-1}, weigh the distances $X - X^b$ and $Y - h(X)$ respectively, and determine the relative contribution of these two distances, in the misfit function. The best dating scenario, i.e., X^a which minimises J, is set as soon as B and R are set. Accordingly, data and glaciological modeling errors must be carefully analysed for each dating problem. It however remains difficult to shape the B matrix, since the errors attached to the glaciological models are poorly known. We give details on the shaping in Appendix 5.

Moreover, we use the approach proposed by Lemieux-Dudon et al., in press, to assess confidence intervals of the best dating scenario $A^{k,a}$, $T^{k,a}$, $C^{k,a}$ and on the associated ice chronologies $\psi^{a,k}$.

3. Application

We applied the new dating method to the EDC, EDML, Vostok and NGRIP cores, to which we assigned indexes $k = 1$, 2, 3, and 4, respectively. In the next sections, we describe the background dating scenarios (Section 3.1) and the glaciological data (Section 3.2).

3.1. Background scenarios

We made use of previously published dating scenarios (except for the NGRIP gas age scale as described in Section 3.1.4). These scenarios are based on either direct or inverse glaciological modeling or on annual layer counting and direct modeling (e.g. NGRIP). The background scenarios based on inverse modeling are already constrained by ice age markers. Strictly speaking, these age markers should not be used again in our application, otherwise we break the classical assumption associated to the Bayesian theorem (i.e., statistical independence between background and observation errors). Nevertheless, we have reused those age markers because they are not numerous compared to the full set of data constraints. The status of the NGRIP background scenario can be seen as distinct from the other cores since the ice chronology relies on annual layer counting.

3.1.1. Vostok background scenario

The Vostok background scenario is denoted $A^{b,1}$, $T^{b,1}$ and $C^{b,1}$. The flow part consists of an inverse local flow model for which the flow parameters are optimised with a Monte Carlo sampling method (Parrenin et al., 2001). The model (Parrenin et al., 2004) enables us to calculate a 2D local velocity field and a Lagrangian backtracing method provides the background ice age estimate $\psi^{b,1}$ (Vk-FGT1 ice age scale). The local flow model is forced by an ice sheet thickness history, which is estimated with the Ritz et al. (2001) 3D thermo-mechanical model. The background accumulation rate $A^{b,1}$ is inferred from three empirical relationships linking: (i) the precipitation rate to the inversion temperature, (ii) the inversion temperature to the mean annual temperature and finally (iii) the mean annual temperature to the isotopic content of ice. Equation (3) enables us to deduce the background thinning function $T^{b,1}$, from the background accumulation rate $A^{b,1}$ and ice age $\psi^{b,1}$. Finally, the background close-off depth $C^{b,1}$ is simulated with Goujon et al. (2003)'s densification model forced by the accumulation rate and temperature histories.

3.1.2. EDC background scenario

The EDC background scenario is written $A^{b,2}$, $T^{b,2}$ and $C^{b,2}$. The ice part is the EDC3model scenario which is simulated with the inverse 1D flow model with Monte Carlo optimised parameters (Parrenin et al., 2007b). Note that the EDC3model scenario differs from the EDC3 reference scenario as mentioned in Section 1. The model error, resulting in part from unresolved physics along with forcing field uncertainties, prevented the Monte Carlo inversion process to verify relevant ice age markers before 41 and after 400 kyr. This problem was solved by subsequently distorting the EDC3model accumulation rate and thinning function, in order that the resulting ice chronology – EDC3 – agrees with the conflicting data (Parrenin et al., 2007a). In this work, when possible, we preferred to use a purely modeled dating scenario as background. The 1D flow model is forced by a conceptual model of ice thickness variations (Parrenin et al., 2007b) tuned to fit the results of Ritz et al. (2001)'s 3D thermo-mechanical model. The background accumulation rate $A^{b,2}$ is inferred from a relationship based directly on the isotopic content of ice. The background thinning function $T^{b,2}$ is deduced from $\psi^{b,2}$ and $A^{b,2}$ with Equation (3). Finally, the sp4 scenario proposed by Loulergue et al. (2007) provides the background close-off depth $C^{b,2}$, which is simulated with the Goujon et al. (2003) densification model.

3.1.3. EDML background scenario

The EDML background scenario is written $A^{b,3}$, $T^{b,3}$ and $C^{b,3}$. The flow simulations are described in Huybrechts et al. (2007). It consists of a local flow model which calculates a 3D velocity field (Pattyn, 2003). A Lagrangian backtracing method enables us to estimate both, the ice age and the total thinning function. A 3D thermo-mechanical model (Huybrechts, 2002) computes the required ice sheet thickness changes and the lateral boundary conditions (note that the background ice age is different from EDML1). The accumulation rate is inferred using the classical empirical relationships with isotopic content (see Section 3.1.1). The Loulergue et al. (2007) sp4 scenario provides the close-off depth, which was simulated with the Goujon et al. (2003) densification model on the basis of EDML1 (Ruth et al., 2007). In the end, the whole modeling exercise provides the EDML background entities $\psi^{b,3}$, $T^{b,3}$, $A^{b,3}$ and $C^{b,3}$.

3.1.4. NGRIP background scenario

The ice part of the NGRIP background scenario relies on GICC05. In addition to the ice chronology $\psi^{b,4}$, GICC05 provides the annual layer thickness $L^{b,4}$. A flow model (Andersen et al., 2004) enables us to estimate the thinning function $T^{b,4}$, and to further deduce the accumulation rate $A^{b,4}$ on the basis of $L^{b,4}$ measurements. In this study, we performed a simulation with the Goujon et al. (2003) densification model in order to estimate $C^{b,4}$. The simulation is run with the following characteristics: (i) the GICC05 ice age scale, (ii) the GICC05 accumulation history and (iii) the mean annual temperature derived from the NGRIP ice isotope measurements ($\delta^{18}O_{ice}$, oxygen-18 of ice, see Johnsen et al. (2001)).

3.2. Glaciological data

We used a total of 1491 chronological markers to constrain the new dating scenarios: ice and gas age markers, ice and gas stratigraphic links and delta-depth estimates. This number is high compared to what has been done previously. The accuracy of the proposed dating depends on the accuracy and density of the applied markers. Most of the markers are concentrated in the time period 0–50 kyr, which explains the fact that our results are tentative beyond 50 kyr.

3.2.1. Ice age markers

A total number of 1034 ice age markers are applied to constrain the Vostok, EDC and NGRIP chronologies (no ice age markers are used to constrain the EDML core).

3.2.1.1. Vostok ice age markers. For the Vostok core, we included the tie points already used to derive the Vk-FGT1 chronology (Parrenin et al. (2004), Table 1 therein). We completed the set with new ice age markers that were estimated on the basis of the inferred relationships between the Vostok local insolation and the Vostok records of O_2/N_2 and air content (Lipenkov et al. in prep, personal communication, 2009).

Table 1
Ice age markers used to constrain the new dating scenario for the Vostok core; the last column specifies the study from which the age markers are extracted: (a) Parrenin et al. (2004), (b) Lipenkov et al. in prep., personal com. 2009.

Age markers	Depth (m)	Age (yr BP)	Uncertainty (yr)	Reference
$^{10}Be/^{14}C$	178	7180	100	(a)
^{10}Be	601	41 000	2000	(a)
Orbital tuning	1904	132 400	6000	(a)
Orbital tuning	2516	200 600	6000	(a)
Orbital tuning	2777	246 000	6000	(a)
Orbital tuning	2945	293 600	6000	(a)
Orbital tuning	3134	336 200	6000	(a)
Orbital tuning	3218	373 800	6000	(a)
Air content – O_2/N_2	2167.5	164 000	800	(b)
Air content – O_2/N_2	2285.5	176 000	400	(b)
Air content – O_2/N_2	2371.5	186 000	600	(b)
Air content – O_2/N_2	2450.5	196 000	1400	(b)
Air content – O_2/N_2	2565	210 000	1200	(b)
Air content – O_2/N_2	2652.5	222 000	200	(b)
Air content – O_2/N_2	2694	230 000	200	(b)
Air content – O_2/N_2	2740.5	240 000	200	(b)
Air content – O_2/N_2	2802	252 000	800	(b)
Air content – O_2/N_2	2858	268 000	200	(b)
Air content – O_2/N_2	2908	282 000	200	(b)
Air content – O_2/N_2	2942.5	290 000	200	(b)
Air content – O_2/N_2	2979	300 000	400	(b)
Air content – O_2/N_2	3027.5	314 000	400	(b)
Air content – O_2/N_2	3071	326 000	400	(b)
Air content – O_2/N_2	3115	336 000	200	(b)
Air content – O_2/N_2	3139	342 000	400	(b)
Air content – O_2/N_2	3169	354 000	600	(b)
Air content – O_2/N_2	3199	368 000	200	(b)
Air content – O_2/N_2	3235	386 000	1500	(b)

3.2.1.2. EDC ice age markers. For the EDC core, we included the age markers used to build the EDC3 ice chronology (Parrenin et al. (2007a), Table 1), but we made several changes to the original set of tie points. First, we used the 36 tie points in Table 1 (Parrenin et al. (2007a), derived from the EDC $\delta^{18}O_{atm}$ record (Dreyfus et al., 2007), as gas age markers instead of ice age markers (see Section 3.2.2). Second, we withdrew two tie points that were inferred from the isotope-methane record synchronisation of the NGRIP and EDML cores during the last deglaciation (respectively at 361.5 and 427.2 m, Parrenin et al. (2007a), Table 1 therein). These two tie points would otherwise introduce redundancy with the EDC-EDML and EDML-NGRIP methane stratigraphic links defined in Section 3.2.4. The final set of ice age markers is summarised in Table 2.

3.2.1.3. NGRIP ice age markers. We selected temporal markers each 60 yr in the temporal window 0–50 kyr directly from the GICC05 ice chronology (not shown, because the resulting data set can easily be deduced from GICC05). The uncertainty of each age marker is chosen as half of the Maximum Counting Error (hereafter *MCE*, see definition in Andersen et al. (2006); Svensson et al. (2008)). This choice is based on the comparisons made by Svensson et al. (2008) and Fleitmann et al. (2009), of GICC05 with other independently dated records in the 0–60 kyr window, showing that most of the records agree with GICC05 within a one σ uncertainty. Strictly speaking, sampling temporal markers each 60 yr probably leads to error correlation between the markers that we did not take into account. In this manner we artificially prevent the GICC05 ice chronology from changing much. In the future, a more rigorous approach would require independent ice age markers (e.g, tephra, speleothems,...) in order to refine GICC05.

Table 2
Ice age markers used to constrain the new EDC core dating scenario. (*): a new mean value of 92.1 ± 0.9 kyr was recently assessed by Dunbar et al. (2008).

Age markers	Depth (m)	Age (yr BP)	Uncertainty (yr)
El Chicon	38.12	691	50
$^{10}Be/^{14}C$	107.83	2716	50
$^{10}Be/^{14}C$	181.12	5280	50
^{10}Be	740.08	41 200	1000
Mt Berlin erupt.(*).	1265.10	92 500(*)	2000(*)
Term. II	1698.91	130 100	2000
Air content	1082.34	70 600	4000
Air content	1484.59	109 400	4000
Air content	1838.09	147 600	4000
Air content	2019.73	185 300	4000
Air content	2230.71	227 300	4000
Air content	2387.95	270 400	4000
Air content	2503.74	313 400	4000
Air content	2620.23	352 400	4000
Air content	2692.69	390 500	4000
Air content	2789.58	431 400	4000
B–M reversal	3165.00	785 000	20 000

3.2.2. Gas age markers

A total number of 49 gas age markers are applied to constrain the EDC and NGRIP chronologies.

3.2.2.1. EDC gas age markers. We relied strictly on Dreyfus et al. (2007) (their Table 1), who derived 36 temporal markers from the $\delta^{18}O_{atm}$ record, by orbital tuning on precession. As a component of the gas phase of ice cores, $\delta^{18}O_{atm}$ provides constraints on gas chronologies (i.e., gas age markers). Because the methodology used by Dreyfus et al. (2007) and Parrenin et al. (2007a) was not designed to optimise the gas chronology but only the ice chronology with ice age markers, they converted the $\delta^{18}O_{atm}$ temporal markers into ice age makers by assessing a delta-age (i.e., the authors applied the EDC2 delta-age). Unlike Parrenin et al. (2007a) and Dreyfus et al. (2007), we applied the set of $\delta^{18}O_{atm}$ data as gas age markers, because our dating method enables to apply both gas and ice age marker constraint and to simultaneously optimise gas and ice chronologies. We set the uncertainty and covariance of uncertainty attached to each age marker to 6000 and 2000 yr, respectively (see Dreyfus et al. (2007) for details).

3.2.2.2. NGRIP gas age markers. Severinghaus et al. (1998) showed that ice isotope and methane in Greenland increase in phase during abrupt climatic transitions. This result is based on measurements of ^{15}N of N_2 (hereafter $\delta^{15}N$), ^{40}Ar, methane and $\delta^{18}O_{ice}$, performed on the GISP2 core, during the Younger Dryas to Pre-Boreal transition (hereafter YD-PB). At this stage, our numerical code is unable to assimilate "stratigraphic links" connecting depths *on the same core*. We therefore cannot rigorously constrain the NGRIP gas age and ice age to be equal during fast climatic transitions recorded in methane and isotopes. To solve this problem, we added 13 gas age markers presented in Table 6, which force the CH_4 and $\delta^{18}O_{ice}$ synchronicity. We assessed a 60 yr uncertainty for the deglaciation transitions and a 100 yr uncertainty for the Dansgaard–Oeschger events (hereafter DO) numbered from 2 to 12.

3.2.3. Ice stratigraphic links

We used a total of 331 ice stratigraphic links to constrain the new dating scenarios. Ice stratigraphic links are defined first between Vostok and EDC, second between EDC and EDML, and finally between EDC and NGRIP.

3.2.3.1. Vostok-EDC ice stratigraphic links. For the last 45 kyr, Udisti et al. (2004) identified 56 major volcanic events that are common to EDC and Vostok (these events are identified from electrical conductivity measurements, hereafter ECM, or from sulfate spikes). We used the pairs of depths (Udisti et al. (2004), their Table 1) as ice stratigraphic links between Vostok and EDC, to which we arbitrarily associated a 200 yr uncertainty. Unlike tephra layers, sulfate or ECM spikes in ice cores are anonymous because they carry no geochemical signature enabling the identication of the eruption and volcanic province. As underlined by Udisti et al. (2004) and Severi et al. (2007), some time intervals show several spikes in one core with no counterpart in the other core. On this basis, we assumed that some depth pairs may have been mismatched. Very careful work should be done to identify uncertain depth pairings in order to better estimate uncertainties. We also extracted three ice stratigraphic links from Narcisi et al. (2005), at logging depths close to 2000 m for both EDC and Vostok (see Table 3). For the latter stratigraphic links, we assumed a logging depth uncertainty of 0.5 m for both EDC and Vostok, leading to an overall root mean square (hereafter RMS) uncertainty of about 100 years.

3.2.3.2. EDC-EDML ice stratigraphic links. Severi et al. (2007) used sulfate spikes to perform an EDC-EDML ice age synchronisation. The related EDC and EDML sulfate profiles were used to transfer the EDC3 ice age scale to the EDML core, resulting in the EDML1 ice age scale (Ruth et al., 2007). We chose 270 of these ice stratigraphic links (according to an index provided by the authors) which defines the quality of the matched volcanic events. We defined an uncertainty ranging from 100 to 300 yr based on this index (see comments in the above paragraph).

3.2.3.3. EDC-NGRIP ice stratigraphic links. A double-peak structure during the Laschamp geomagnetic excursion around 41 kyr, was identified in the ^{10}Be records of GRIP (Yiou et al., 1997) and EDC (Raisbeck et al., 2007). The transfer of the ^{10}Be peaks from GRIP to NGRIP relies on a match of the GRIP and NGRIP $\delta^{18}O_{ice}$ records. The matching is precise because the two ^{10}Be peaks are contemporary to DO 10, and we assigned an arbitrary 50 yr synchronisation error. In addition, Loulergue et al. (2007) provided uncertainties on the depth of the ^{10}Be peaks in the NGRIP and EDC cores, which we converted into temporal uncertainties, according to the NGRIP and EDC background age scales. The resulting RMS error is about 110 years (Table 4).

3.2.4. Gas stratigraphic links

The gas stratigraphic links applied to constrain the new dating scenarios are defined between Vostok and EDC, EDC and EDML and EDML and NGRIP (a total number of 50 markers).

3.2.4.1. Vostok-EDC gas stratigraphic links. We derived 5 gas stratigraphic links during the last and the penultimate deglaciation by matching the methane records of Vostok (Petit et al., 1999) and EDC (Loulergue et al., 2008) (Table 5).

3.2.4.2. EDC-EDML gas stratigraphic links. The set of 24 gas stratigraphic links between EDC and EDML are derived from the matching of methane records proposed by Loulergue et al. (2007), Table 2 therein.

3.2.4.3. EDML-NGRIP gas stratigraphic links. We derived a set of 21 gas stratigraphic links by matching the EDML and Greenland CH_4 records for each onset and termination of the fast transitions, from the onset of the Holocene back to 50 kyr. We inferred a 100 year synchronisation uncertainty (2σ) except for the initial slow methane rise of DO 1 and for the DO 2,3 and 4, for which we assessed errors between 130 and 160 years (Table 7).

Table 3
Ice stratigraphic links derived from common volcanic events identified through geochemical analysis of tephra layers that are inventoried in Narcisi et al. (2005). Note that all the Vostok depths are transferred to core 3G, e.g., ash layers at 1996.3 and 2586.15 m depth, along the cores $4G_2$ and $5G_1$, are transferred to the core 3G at 2000.70 and 2589.56 m depth, respectively. At 2 km depth, we assumed a logging depth uncertainty of 0.5 m, roughly equivalent to 50 and 100 years for Vostok and EDC, respectively. The resulting RMS error is around 100 yr.

	EDC depth (m)	Vostok depth (m)	Uncertainty (yr)
Ash layer	1804.0	2000.70	100
Ash layer	2086.6	2501.92	100
Ash layer	2150.9	2589.56	100

Table 4
Ice stratigraphic links derived from the double-peak structure of GRIP-EDC ^{10}Be records (see Loulergue et al. (2007)). Uncertainties in m are converted into temporal uncertainties, according to the NGRIP and EDC background age scales, with a resulting RMS error of about 110 years.

	EDC depth (m)	NGRIP depth (m)	Uncertainty (yr)
Peak 1	735.5 ± 1.1	2110.1 ± 1.1	110
Peak 2	744.8 ± 1.1	2127.5 ± 1.1	111

3.2.5. Delta-depth markers

3.2.5.1. Vostok delta-depth markers. We used the two delta-depth estimates (63 ± 7 m at 1503.33 m and 20 ± 2 m at 2784 m) proposed by Caillon et al. (2001); Caillon et al. (2003), for transition 5d/5c and termination III, respectively (these estimates being assessed on the basis of $\delta^{15}N$, $\delta^{40}Ar$ and ice isotopic measurements).

3.2.5.2. EDC delta-depth markers. For termination I and II, we used the delta-depth estimates with uncertainties proposed by Dreyfus Boissier (2008) on the basis of $\delta^{15}N$ and ice isotopic measurements. In addition, we added a set of 17 delta-depth markers with uncertainties defined in Dreyfus et al. (2007) (Table 2, therein). Those latter estimates were deduced from warming or cooling events which were assumed to be simultaneously recorded in the gas phase (CO_2 and CH_4) and in the ice matrix (ice isotopes). A more rigorous work would require us to assess and introduce a time shift, which is known to occur between the greenhouse gas and ice isotopic signals (Caillon et al., 2003). This would lead to apply different delta-depth values or to introduce error correlations between the delta-depth markers.

3.2.5.3. NGRIP delta-depth markers. We used the delta-depth estimates proposed by Huber et al. (2006) for DO 9 to 12, on the basis of $\delta^{15}N$, $\delta^{40}Ar$ and ice isotopic measurements (16.29 ± 1.5, 15.39 ± 1.5, 15.01 ± 2 and 11.85 ± 1.5 m at 2099.90, 2124.10, 2157.65, and 2222.00 m, respectively, A. Landais, personal communication).

4. Results and discussion

First, we give an overview of the new dating scenarios (Section 4.1). We restrict ourselves to the EDC and EDML cores, because at this stage of the study, too few data are used to constrain the Vostok chronologies, and moreover we "artificially" limited the possibility of change in the NGRIP gas age scale (see Section 3.2.1). We subsequently present the methane and ice isotope records, according to the new dating scenarios, on the well-constrained period from present-day back to 50 kyr, and discuss the new North-

Table 5
EDC-Vostok gas stratigraphic links derived from methane records during the last and the penultimate deglaciation; YD–PB = Younger Dryas to Pre-Boreal; BA–YD = Bolling–Allerod to Younger Dryas; GL–BA = Glacial to Bolling–Allerod; TII = Termination II.

	EDC depth (m)	Vostok depth (m)	Uncertainty (yr)
YD–PB	418.2	319.96	150
BA–YD	442.7	346.16	150
GL–BA	476.1	372.2	150
TII	1722	1852.1	300
TII	1770	1879.7	300

Table 6
NGRIP depth and GICC05 age of the major rapid climate changes, as recorded in the ice isotope. The GICC05 ice age of each event is attributed to each corresponding methane events, and provide a gas age marker. YD–PB = Younger Dryas to Pre-Boreal; GL–BA = Glacial to Bolling–Allerod; DO = Dansgaard–Oeschger event.

	NGRIP depth (m)	age (yr)	Uncertainty (yr)
YD–PB	1516.37	11 760	60
GL–BA	1638.01	14 740	60
DO2	1824.08	23 440	100
DO3	1897.12	27 860	100
DO4	1911.63	28 920	100
DO5	1969.62	32 580	100
DO6	1994.17	33 880	100
DO7	2027.61	35 600	100
DO8	2087.90	38 360	100
DO9	2119.17	40 200	100
DO10	2142.27	41 500	100
DO11	2175.27	43 480	100
DO12	2239.68	46 900	100

South timing, in particular during the last deglaciation (Section 4.2). Finally in Section 4.3, we analyse the reconstructed accumulation rate, close-off depth and thinning function, in order to validate the new dating scenarios between 0 and 50 kyr.

4.1. EDC and EDML new ice and gas chronologies and confidence intervals

Figs. 2 and 3 present the overall new ice and gas chronologies, in comparison with the background chronologies, for the entire EDC and EDML cores, respectively. Also shown is the uncertainty (2σ) relevant to the new ice age scales, as well as the delta-depth reconstructions and the data constraints. Figs. 4 and 5 present the same curves, but using the 0–20 kyr temporal window.

As can be noted from these figures, the new dating scenarios are in agreement with the data constraints. Moreover, on Fig. 3, one can note that the delta-depth reconstruction for EDML is in agreement with the values assessed by Loulergue et al. (2007), on the basis of the EDC and GRIP ^{10}Be records. A possible underestimation of the uncertainty attached to the EDC delta-depth proposed by Loulergue et al. (2007) may explain a slight disagreement with our delta-depth reconstruction for EDC (see Fig. 2).

Table 7
Gas stratigraphic links derived from the match of the EDML CH_4 record with the Greenland CH_4 stack record from present back to 55 kyr BP. YD–PB = Younger Dryas to Pre-Boreal; BA–YD = Bolling–Allerod to Younger Dryas; GL–BA = Glacial to Bolling–Allerod; DO = Dansgaard–Oeschger event.

Transitions	NGRIP depth (m)	EDML depth (m)	Uncertainty (yr)
YD–PB	1511.54	716.55	100
BA–YD	1540.08	767.19	100
GL–BA	1627.89	827.53	100
Slow raise	1673.15	905.30	160
DO3 end	1796.95	1044.32	130
DO3 onset	1818.63	1070.99	160
DO2 end	1879.28	1149.2	130
DO2 onset	1891.96	1152.90	130
DO4 end	1901.97	1165.33	130
DO4 onset	1909.45	1173.42	100
DO5 end	1954.86	1224.54	100
DO5 onset	1963.88	1233.39	100
DO6 end	1981.94	1248.48	100
DO6 onset	1991.88	1260.59	100
DO7 end	2003.66	1272.56	100
DO7 onset	2024.93	1286.72	100
DO8 end	2042.86	1311.85	100
DO8 onset	2086.67	1337.84	100
DO9 onset	2115.88	1373.84	130
DO10 end	2125.12	1391.77	100
DO10 onset	2141.01	1404.59	100
DO11 end	2149.46	1417.60	100
DO11 onset	2173.20	1441.59	100
DO12 end	2185.66	1451.82	100
DO12 onset	2236.86	1490.22	100

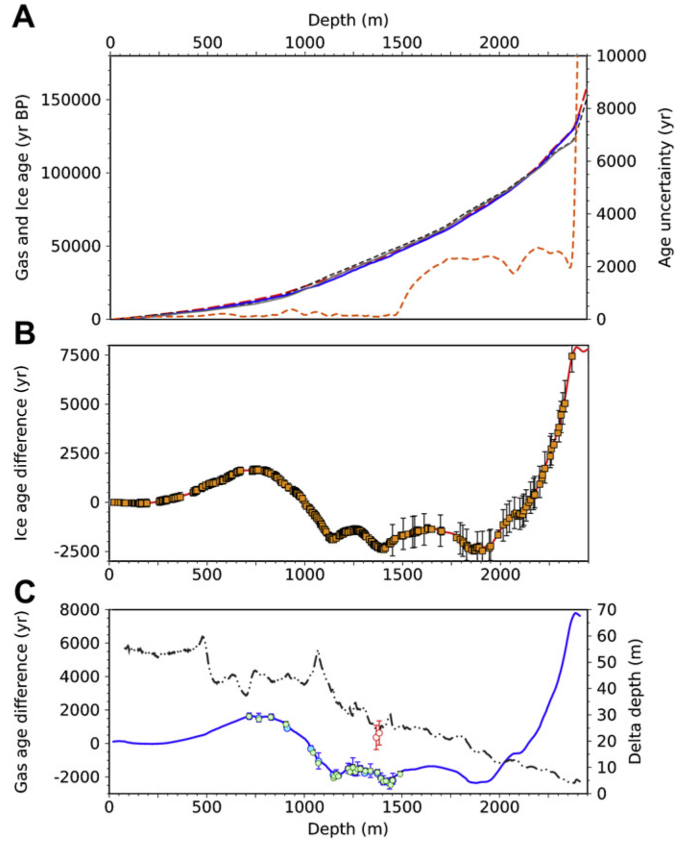

Fig. 2. EDC overall new dating scenario for ice and gas: (A) New and background ice and gas chronologies and uncertainty on the ice age estimate (orange dashed line, right Y-axis). Ice chronologies are dashed lines while gas chronologies are solid lines; background chronologies are in dark grey while new ice and gas chronologies are red and blue lines, respectively. (B) Difference between new and background ice age scales (i.e., new minus background, red line); red triangles are ice age markers; orange squares, orange and green diamonds are EDC-EDML, EDC-Vostok and EDC-NGRIP ice stratigraphic links, respectively; error bars correspond to 2σ uncertainties. (C) Difference between new and background gas age scales (blue line); new delta-depth reconstruction (black dashed line, right Y axis); blue triangles are gas age markers; blue and purple circles are respectively EDC-EDML and EDC-Vostok gas stratigraphic links; red circles are delta-depth data inferred by Loulergue et al. (2007), which are not used to constrain the new dating scenarios but are plotted for comparison; error bars are 2σ uncertainties.

Figs. 2–5 confirm that the method presented can be applied on several cores simultaneously, on large depth intervals and with numerous chronological data of different types. They also show that the uncertainties assessed for the new ice age scales behave as expected: a growing trend with depth and superimposed drops in the neighbourhood of data. All these results constitute a real dating improvement, as compared with to the performance of either direct or inverse glaciological modeling that has been used for dating purposes to date.

4.2. Methane and ice isotope records: new North-South timing

4.2.1. Matching the methane records

On the time window 7–20 kyr, the EDC, EDML and Greenland methane records are shown on panel A in Fig. 6, according to the new dating scenarios. In comparison with the current gas age

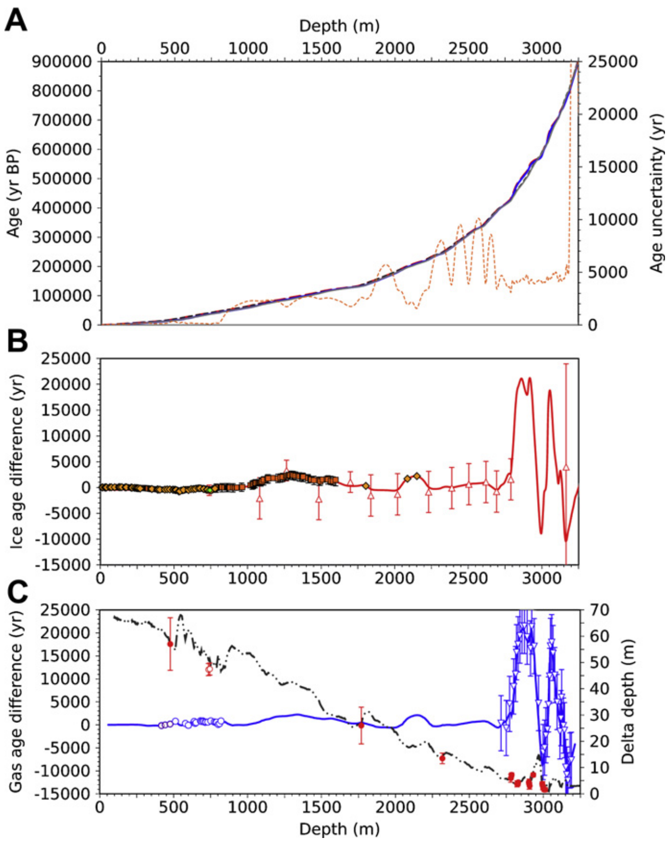

Fig. 3. EDML overall new dating scenario for ice and gas: (A) New and background ice and gas chronologies and uncertainty on the ice age estimate; see Fig. 2 for plot symbols. (B) Difference between new and background ice age scales (i.e., new minus background, red line); orange squares are EDML-EDC ice stratigraphic links; error bars correspond to 2σ uncertainties. (C) Difference between new and background gas age scales (blue line); new delta-depth reconstruction (black dashed line, right Y axis); blue and green circles are EDML-EDC and EDML-NGRIP gas stratigraphic links, respectively; red filled circles are delta-depth data; red empty circles are delta-depth inferred by Loulergue et al. (2007) but unused in the application; error bars are 2σ uncertainties.

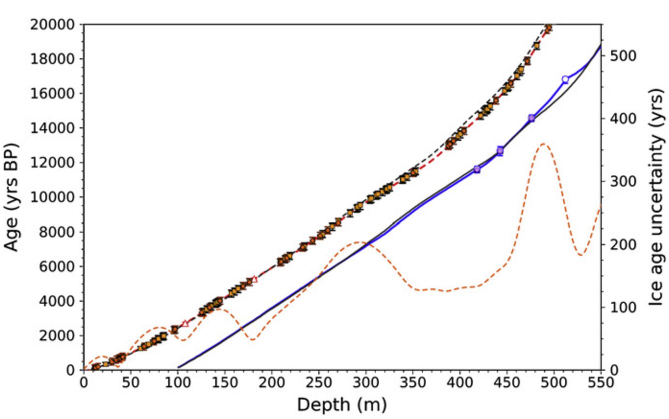

Fig. 4. EDC new ice and gas chronologies with uncertainty, compared to the background chronologies on a 0–20 kyr temporal window. Ice chronologies are dashed lines while gas chronologies are solid lines; the background chronologies are in dark grey while the new ice and gas age are red and blue lines, respectively; the confidence interval (2σ) is plotted as orange dashed line (right Y-axis); ice age markers are red triangles; orange squares and diamonds are EDC-EDML and EDC-Vostok ice stratigraphic links, respectively; blue and purple circles are EDC-EDML and EDC-Vostok gas stratigraphic links, respectively; error bars are 2σ uncertainties.

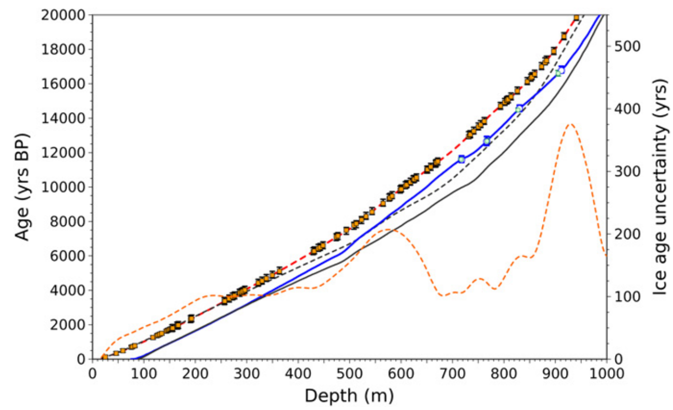

Fig. 5. EDML new ice and gas chronologies with uncertainty, compared to the background chronologies on a 0–20 kyr temporal window. See Fig. 4 for plot symbols; orange diamonds are EDML-EDC ice stratigraphic links; blue and green circles are EDML-EDC and EDML-NGRIP gas stratigraphic links, respectively; error bars are 2σ uncertainties.

scenarios shown on panel A in Fig. 1, the new gas scenarios resolve the mismatch during the deglaciation. The matching of the Greenland and Antarctic methane records also holds for the DO events and DO like-events from 2 to 12 (not shown).

During the Glacial to Bolling–Allerod transition (hereafter GL–BA), the new NGRIP gas age is about 200 years younger than the gas chronology proposed by Blunier et al. (2007). The abrupt rise of the Greenland methane stack record starts and stops at 14 700 and

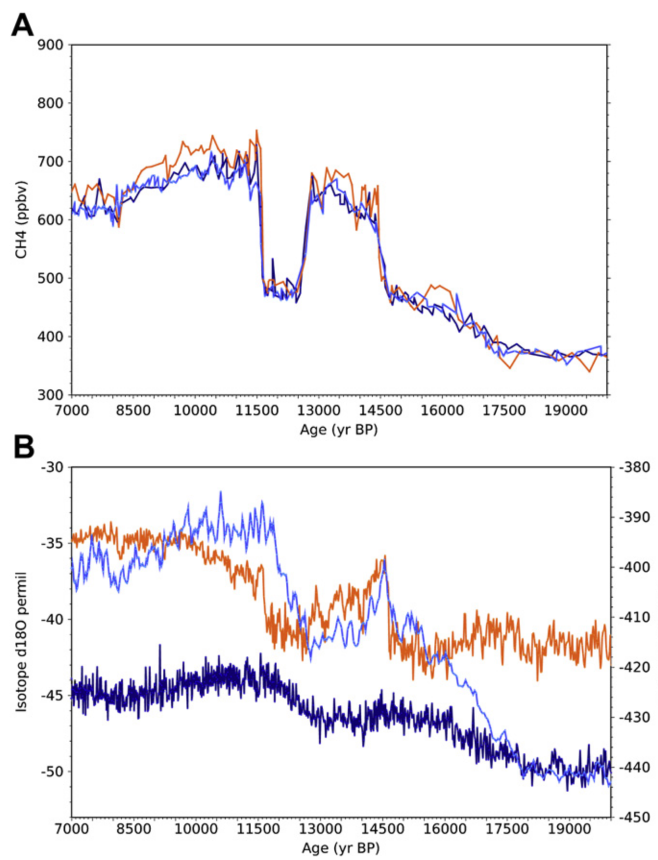

Fig. 6. New ice and gas chronologies for the EDC and EDML cores (light and dark blue lines, respectively) and for the NGRIP core (orange line), during the last deglaciation: (A) methane records; (B) ice isotope records.

14 450 yr before present (BP) respectively (where present is defined as 1950 AD), which falls within the uncertainty estimated by Blunier et al. (2007). Our results also suggests that the EDC3gas_a and EDML1gas_a (i.e., the sp4 scenario) are respectively 450 and 150 years too young, during the GL–BA, and that EDC3gas_a is 350 and 300 years too young during the Bolling–Allerod to Younger Dryas (hereafter BA–YD) and YD–PB transitions, respectively.

4.2.2. North-South timing as recorded in the ice isotope records

The climatic transitions as recorded in the Greenland and Antarctic ice isotopic records (the EDC δD record, Jouzel et al. (2007), the EDML $\delta^{18}O_{ice}$ record, EPICA Community Members (2006) and the NGRIP $\delta^{18}O_{ice}$, Johnsen et al. (2001)) are plotted against the new dating scenarios on panel B in Fig. 6, as well as on panel A in Fig. 7, on the time intervals 7–20 kyr and 30–50 kyr, respectively. The panel B in Fig. 7 shows the latter records according to EDC3, EDML1 and GICC05, for comparison.

Comparison of Figs. 1 and 6, panels B, suggests that the EDC3 and EDML1 ice chronologies are both too young during the GL–BA and YD–PB transitions. According to the new dating scenarios, the end of the GL–BA transition should be shifted towards older ages by 300 yr for EDC and 250 yr for EDML. Meanwhile, for the end of the BA–YD transition, the shifts towards older ages should be 125 and 75 yr for EDC and EDML, respectively. On the basis of our results, we propose a new dating for the warming in Antarctica during the last deglaciation, with the onset and end dated to 17 900 ± 300 and 14 550 ± 130 yr BP (see the 2σ uncertainty plotted on Fig. 4), instead of 17 400 and 14 250 yr BP.

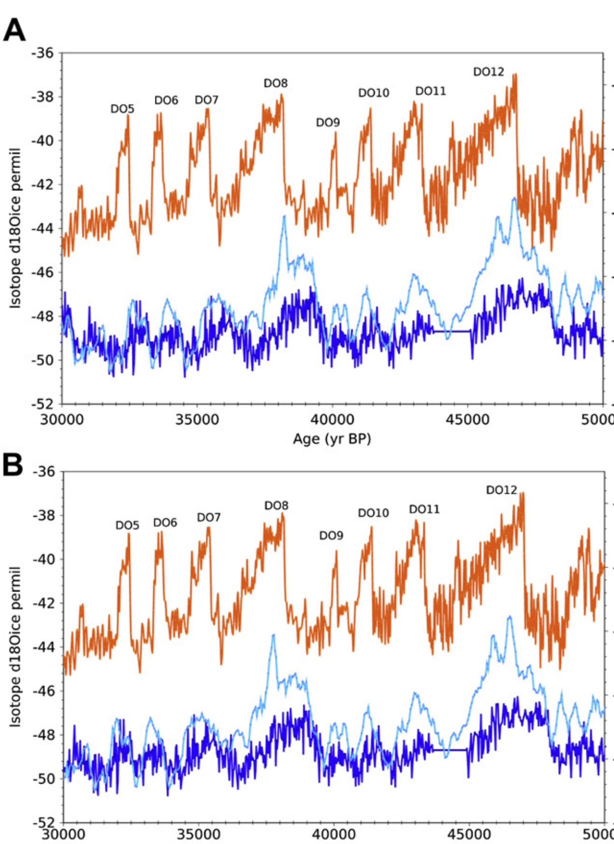

Fig. 7. EDC δD (light blue), EDML (dark blue) and NGRIP (orange) δ^{18}O ice isotope records, on the time interval 30–50 kyr: (A) plotted against the new dating scenarios (this work); (B) plotted against the EDC3, EDML1 and GICC05 ice age scales. The DO events (i.e., Dansgaard–Oeschger) and Antarctic counterparts are shown and the new timing for the major DO, e.g., 8 and 12, is underlined.

At last, as shown on Fig. 7, the timing between the Greenland DO events and the Antarctic DO like-events from 5 to 12 is also modified. These changes lead to new dating scenarios in better agreement with the bipolar see-saw concept (Stocker, 1998; Blunier and Brook, 2001; EPICA Community Members, 2006), not only for the last deglaciation transitions but also for the major DO and DO-like events, e.g., DO 8 and 12. The new timing for the DO 2, 3, 4 and 11 should not be considered here because the stratigraphic links between the EDML methane record and the Greenland methane stack record are imprecise (the EDML record is noisy for DO 2, 3 and 4) or non existent (there is a gas in the EDML record for DO 11).

4.3. Analysis of the reconstructed glaciological entities

4.3.1. Corrections to the modeled accumulation, thinning and close-off depth

Fig. 8 displays the ratios between the new and the background accumulation rate, thinning function and close-off depth for EDC and EDML. These ratios are corrections relative to the background scenarios (see Section 3.1). In the time window 0–40 kyr, the corrections are in agreement with the modeling errors expected for the corresponding glaciological entities.

The corrections applied to the EDC modeled thinning function are very small (a maximum correction of 5%). They are in agreement with ice flow modeling uncertainties expected in the top part of domes. For EDML, the latter corrections are larger (close to 18%

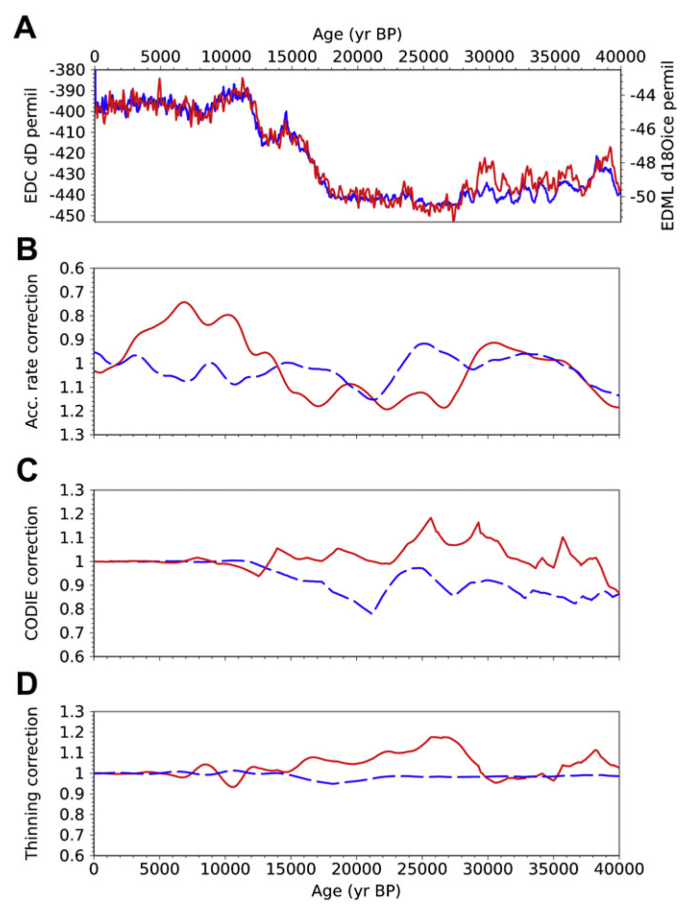

Fig. 8. EDC (blue/dashed blue) and EDML (red) climatic records and correction on glaciological entities, plotted against the new chronologies: (A) Ice isotope records; (B) Ratio between the new and background accumulation rate (reverse Y-axis); (C) Ratio between the new and background close-off depth (labelled "CODIE correction" to refer to the measurement unit "m-ie", i.e., meters of ice equivalent); (D) Ratio between the new and background thinning function.

between 25 and 28 kyr possibly due to the low density of constraints). Such results are consistent with the EDML drilling location down-stream on a flow line, which implies that both temporal and spatial variations of the forcing fields must be assessed in the modeling, conversely to EDC.

The corrections applied to the close-off depth expressed in meters of ice equivalent, do not exceed 22% for both EDC and EDML. These corrections are consistent with the typical variations of modeled and measured close-off depths (Goujon et al., 2003; Landais et al. (2006a); Loulergue et al., 2007), particularly when the related changes in the firn density profiles are considered. A discussion on the reconstructed EDC close-off depth is detailed in Section 4.3.3.

The corrections applied to the modeled accumulation rate directly provides the multiplying factors (varying with depth and time), to apply to the accumulation model, i.e., the classical relationship with the ice isotope. Some overall larger corrections are calculated for EDML, in comparison with EDC, with a maximum correction of 26% during the Holocene. One can note that the shape of the inverse correction, apart from its timing, is similar to the trend of the climatic signal during the deglaciation transitions and the early Holocene. The new EDML accumulation rate scenario is discussed in the following section.

4.3.2. Accumulation rate reconstructions

Fig. 9 compares the new and the background scenarios for the EDML accumulation rate. It also shows the EDC and EDML ice isotopic records plotted against the new ice age scales, as well as the reconstructed accumulation rate for EDC.

The resulting new EDML accumulation scenario shows little resemblance with the ice isotopic signal, especially between 3 and 11 kyr. The new scenario does not predict high values for the early Holocene optimum and the accumulation is lower than predicted by the classical relationship with the isotope. Such a difference seems likely, as EDML site stands along a flow line. The Holocene ice originates up to 20 km upstream (Huybrechts et al., 2007). Moreover, large spatial variabilities in accumulation are observed in the neighbourhood of the EDML drilling site, close to 20% on the 30 km traverse between DML05 (B32 drilling) and DML19 sites (Oerter et al., 2000). Rotschky et al. (2004) also reported changes in accumulation rate varying from 45 to 65 kg m$^{-2}yr^{-1}$ eastwards of point DML05, along the ice divide, and some accumulation spots below 45 and above 85 kg m$^{-2}yr^{-1}$. On this basis, the temporal variability of processes affecting the accumulation pattern may also explain the low reconstructed rates in the 4–11 kyr period: (i) Wind-scouring known to occur in the area, may have triggered snow redistribution mechanisms, (ii) large scale or regional changes in the air mass advection during the Holocene are also possible, and (iii) both mechanisms may be responsible for changes in the previous ice divide location.

We must however remain cautious regarding the EDML accumulation rate reconstruction. The corrections to the accumulation rate and the distortion of the ice age scale (see Equation (3)) are dependent: inaccurate data constraints may result in inaccurate accumulation corrections. One has therefore to question the set of chronological data used to constrain the new dating scenario. The EDML ice chronology is tightly linked to the EDC ice chronology by means of stratigraphic links derived from volcanic sulfate spikes. Udisti et al. (2004) mentioned that only a few common volcanic spikes can be unambiguously identified during the last deglaciation. They underlined the existence of a reliable triplet of sulfate spikes at 390 m depth in the EDC core (i.e., around 13 kyr on the new ice age scenario). In our application, we included as stratigraphic links, the reliable triplet mentioned above, but also other pairs of common sulfate spikes proposed by Udisti et al. (2004) for EDC and EDML. The uncertainties assessed for the latter stratigraphic links might have been underestimated. To solve this issue and refine the proposed accumulation rate scenario, other stratigraphic links such as tephra layers might be considered, as well as proxies of accumulation changes such as chemical records.

4.3.3. Delta-age and close-off depth reconstructions

Fig. 10 shows the delta-age and delta-depth reconstructions for the EDC core, as estimated with three different scenarios: (i) the sp1 scenario (Loulergue et al., 2007) built with the (Goujon et al.,

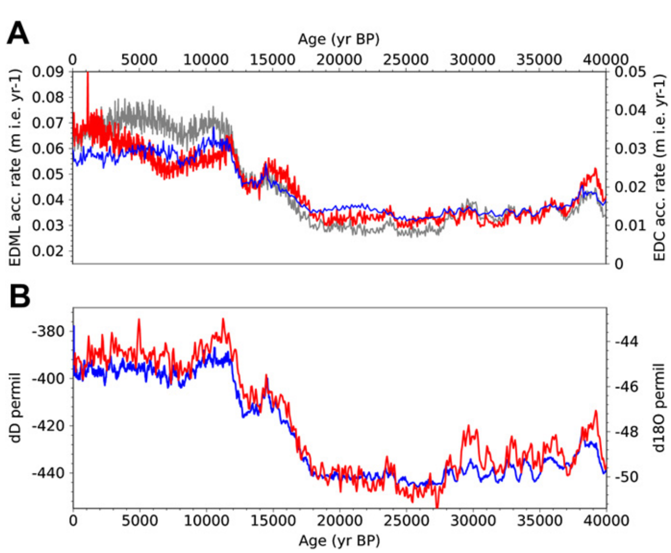

Fig. 9. New EDC and EDML accumulation rate reconstructions and isotope records, plotted against the new chronologies: (A) New EDML (red, left Y-axis) and new EDC accumulation rate (blue, right Y-axis) compared to the background EDML accumulation (grey, left Y-axis). (B) New EDML $\delta^{18}O_{ice}$ record (red) and EDC δD record (blue).

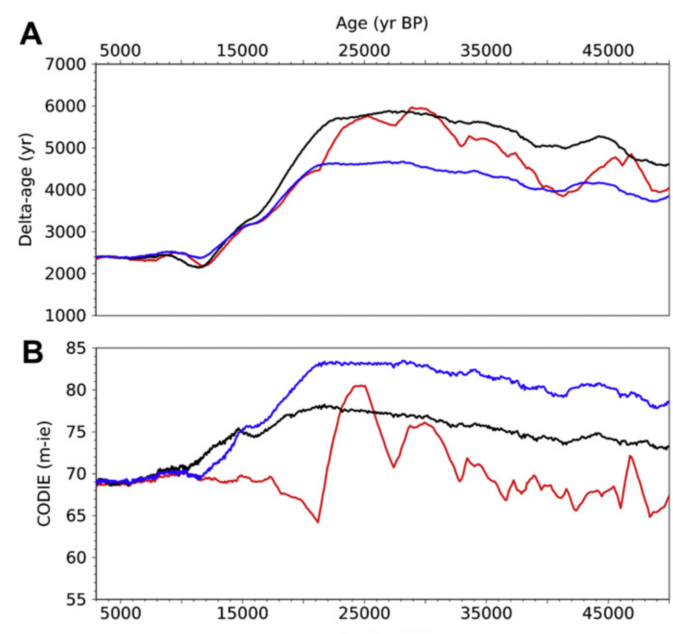

Fig. 10. Comparison of the EDC delta-age and close-off depth scenarios for the last 50 kyr: (A) Delta-age scenarios: sp1 scenario (black), sp4 scenario (blue) and the present work scenario (red). (B) Close-off depth scenarios (labelled "CODIE" to refer to the measurement unit "m-ie", i.e., meters of ice equivalent): sp1 scenario (black), sp4 scenario (blue) and the present work scenario (red).

2003) densification model on the basis of an accumulation rate history, which is consistent with the EDC3 age scale, (ii) the sp4 scenario (Loulergue et al., 2007) (see Section 1) and (iii) the new dating scenario.

Panel A in Fig. 10 confirms that the sp1 scenario overestimates the EDC delta-age, as observed by Loulergue et al. (2007). The delta-age behaviour in the 22–32 kyr time interval cannot be discussed, due to the poor quality of the data constraints. Conversely, in the neighbourhood of the Laschamp excursion (41 kyr), the gas and ice ages are both well-constrained (see Section 3.2.3) and yield good confidence.

On panel B in Fig. 10, the new EDC scenario assesses a thinner close-off depth (denoted CODIE on Fig. 10) than simulated by the densification models during the glacial periods. The high close-off depth values estimated by densification models have already been questioned by δ^{15}N measurements in Antarctica (Landais et al., 2006a). Further studies are however necessary in order to settle the issue. From the gravitational fractionation of δ^{15}N in firn, the depth of the diffusive column can be assessed. However, our poor knowledge of the convective and non-diffusive zones in Antarctic firn during glacial periods (up to 40 m, A. Landais, personal communication) makes it difficult to deduce an accurate close-off depth (sum of convective, non-diffusive and diffusive zones) from δ^{15}N measurements (Caillon et al. (2003); Landais et al. (2006a), Dreyfus et al., this issue).

5. Summary and further prospects

A new dating method based on inverse techniques allows calculating consistent gas and ice chronologies for several ice cores on large depth intervals. The method enables us to cross-constrain the age scales with global or regional stratigraphic markers. It provides the best compromise between the constraints brought by glaciological models and data. It does not improve the description of the glaciological models (ice flow models and/or firn densification models), but it refines the existing dating scenarios of accumulation rate, thinning function and close-off depth, and it provides improved gas and ice age chronologies in agreement with the glaciological data. At the same time, an age uncertainty is estimated on the basis of the probabilistic formulation of the method.

We applied this method to four ice cores at the same time, Vostok, EDC, EDML and NGRIP, using background dating scenarios provided by the literature. We proved the method able to be applied simultaneously to several Greenland and Antarctic cores and to produce new dating scenarios in agreement with several chronological constraints.

We focused on time intervals that were properly constrained with gas and ice temporal markers, stratigraphic links and delta-depth measurements. In the time interval 0–50 kyr and particularly during the last deglaciation, we improved the overall gas and ice age consistency and reconciled the Greenland and Antarctic methane records. We also suggested that the EDC3 reference chronology is too young during the last deglaciation.

In addition, we analysed the differences between the new and pre-existent scenarios of accumulation rate, thinning function and close-off depth, and the new values are kept within the limits of physical mechanisms. Our application however supports the idea that during glacial periods and for cold sites such as EDC, the close-off depth may be smaller than predicted by densification models. Moreover, the EDML accumulation rate reconstructions question the accumulation rate model accuracy and/or the reliability of the volcanic sulfate matching during the Last Glacial Maximum to Holocene transition. In this respect, the search for additional stratigraphic links such as tephra layers would help solve this issue.

The new dating method (as well as the proposed dating scenarios between 0 and 50 kyr) opens perspectives for perfecting the interpretation of paleoclimate records. In particular, the timing between Antarctic and Greenland climate (as recorded in the ice isotope) confirms the concept of an underlying see-saw mechanism. In the future, the method may provide some insights both on the sources of inaccuracy of the forward glaciological models, and on the origins of the glaciological data variability (e.g., firn properties, ice isotope, δ^{15}N, ice microstructure and fabric, etc.), by analysing the differences between the new and pre-existent scenarios of accumulation rate, thinning function and close-off depth, and by comparing them with the paleo-records. For the layer counted age scales, such analysis may help to identify inaccurate determinations of annual layer thickness (for instance during cold periods with thin annual layers).

The new dating method proves to be a very useful tool, combining widespread chronological information in order to calculate consistent ice core chronologies. However, the reliability of the chronologies calculated by this means depend on the quality and accuracy of the chronological constraints. It is therefore of importance to: (i) carefully choose the data incorporated in the dating process, as well as the background dating scenarios, (ii) carefully estimate the associated uncertainties and (iii) cautiously analyse the results. This method offers perspectives in the field of paleoclimatology and could be extended for applications to marine and continental cores.

Acknowledgement

We choose to dedicate this work to our friend and colleague Jean-Marc Barnola, who passed away September 21, 2009. Discussions with Emilie Capron, Amaëlle Landais, Mickael Town, Gaël Durand, Olivier Gagliardini, Gabrielle Dreyfus, Valérie Masson and Jean Jouzel were very helpful in the construction. We are also grateful to Michel Sacchettini for his technical help and to Volodya Lipenkov and Dominique Raynaud for providing new Vostok age markers based on the comparison of air content and O_2/N_2 records. We acknowledge the reviewers and the editor Hubertus Fischer, for their useful comments, suggestions and corrections.

This work was supported by the Agence Nationale de la Recherche (projects ANR-05-BLAN-0165-01 and ANR-07-BLAN-0125). It is a contribution to the European Project for Ice Coring in Antarctica (EPICA), a joint European Science Foundation/European Commission scientific programme, funded by the EU and by national contributions from Belgium, Denmark, France, Germany, Italy, the Netherlands, Norway, Sweden, Switzerland and the United Kingdom. The main logistic support was provided by IPEV and PNRA (at Dome C) and AWI (at Dronning Maud Land). This is an EPICA publication no. 246.

Appendix. Background error covariance matrix

The B matrix is defined as $B = E[(\epsilon^b)(\epsilon^b)^T]$, ϵ^b is the euclidean distance between X^t and X^b, the true and background dating scenarios, respectively.

Defining very precisely the B matrix is of course out of reach in practical applications, since X^t is unknown. However, there are different means of getting some insights on B. One can for instance perform a statistical analysis, comparing the glaciological dating scenarios built with simple flow models for dating purposes, to the ones simulated with more complex flow models. Such a statistical analysis is not in the scope of this paper and we only use a very preliminary shaping of the B matrix.

We assume no error correlation between the background entities of two distinct ice cores. We further assume no error correlation between $A^{b,k}$, $T^{b,k}$ and $C^{b,k}$. The B matrix is therefore made of diagonal blocks B^k, where each block related to the core k is written:

$$B^k = \begin{pmatrix} B_{A^{b,k}} & 0 & 0 \\ 0 & B_{T^{b,k}} & 0 \\ 0 & 0 & B_{C^{b,k}} \end{pmatrix} \tag{A1}$$

We independently set $\sigma^{b,k}$, the standard deviation vectors and $\rho^{b,k}$, the correlation matrices associated with the three sub-matrices $B_{A^{b,k}}$, $B_{T^{b,k}}$ and $B_{C^{b,k}}$:

$$\left[B_{A^{b,k}}\right]_{ij} = \left[\sigma_A^{b,k}\right]_i \left[\sigma_A^{b,k}\right]_j \left[\rho_A^{b,k}\right]_{ij} \tag{A2}$$

$$\left[B_{T^{b,k}}\right]_{ij} = \left[\sigma_T^{b,k}\right]_i \left[\sigma_T^{b,k}\right]_j \left[\rho_T^{b,k}\right]_{ij} \tag{A3}$$

$$\left[B_{C^{b,k}}\right]_{ij} = \left[\sigma_C^{b,k}\right]_i \left[\sigma_C^{b,k}\right]_j \left[\rho_C^{b,k}\right]_{ij} \tag{A4}$$

We define the $\rho_{A^{b,k}}$ and $\rho_{C^{b,k}}$ correlation matrices as functions of *age differences* while the $\rho_{T^{b,k}}$ matrix is set as a function of *depth differences*. This separation is based on the distinct dependence of $A^{b,k}$ and $T^{b,k}$ either on age or on depth. Changes in accumulation rate are not linked to the drilling depth but more naturally to the paleoclimate change through time. The total thinning of an ice layer is more intrinsically a mechanical state attached to the depth of the layer.

The error variance on $A^{b,k}$ (resp. $C^{b,k}$) is assumed to depend on the product of $\sigma_{A,0}{}^{b,k}$ (resp. $\sigma_{C,0}{}^{b,k}$) a scalar parameter, and the normalized squared distance between the past and present-day site temperature (i.e., the further we are from present-day climate the greater the uncertainty on background accumulation rate and close-off depth). $\sigma_{A,0}{}^{b,k}$ (resp. $\sigma_{C,0}{}^{b,k}$) is set equal to 0.5. The correlation matrix $\rho_A^{b,k}$ (resp. $\rho_C^{b,k}$) is defined as a Gaussian distribution of $\psi^{b,k}$, which depends on $L_A^{b,k}$ (resp. $L_C^{b,k}$), a correlation length parameter in time unit set to 4000 yr. $\rho_A^{b,k}$ (resp. $\rho_A^{b,k}$) is therefore written:

$$\begin{aligned} \left[\rho_A^{b,k}\right]_{ij} &= \exp\left[-\frac{1}{2}\left(\frac{\psi_i^{b,k}-\psi_j^{b,k}}{L_A^{b,k}}\right)^2\right] \\ \left[\rho_C^{b,k}\right]_{ij} &= \exp\left[-\frac{1}{2}\left(\frac{\psi_i^{b,k}-\psi_j^{b,k}}{L_C^{b,k}}\right)^2\right] \end{aligned} \tag{A5}$$

The error variance on $T^{b,k}$ is chosen in order to agree with the following comment: the longer the ice particle trajectories, the greater is the error of the forward model. One candidate for $\sigma_T^{b,k}$, the error variance vector, can therefore be a growing function of the inverse of $T^{b,k}_i$ (the total thinning experienced by the ice layer between depths z^k_{i-1} and z^k_i):

$$\left[\sigma_T^{b,k}\right]_i = \sigma_{T,0}^{b,k}\left[\frac{1}{10} + \frac{1}{H}\sum_{j=1}^{i}\frac{dz_j^k}{T_j^{b,k}}\right] \tag{A6}$$

where H is the total ice thickness and $\sigma_{T,0}{}^{b,k}$ a parameter which is set to 0.45. The related correlation profile is here again chosen as a Gaussian distribution with an associated correlation length parameter $L_T^{b,k}$ set to 70 m:

$$\left[\rho_T^{b,k}\right]_{i,j} = \exp\left[-\frac{1}{2}\left(\frac{z_i - z_j}{L_T^{b,k}}\right)^2\right] \tag{A7}$$

References

Alley, R.B., Brook, E.J., Anandakrishnan, S., 2002. A northern lead in the orbital band: north-south phasing of Ice-Age events. Quaternary Science Reviews 21 (1–3), 431–441.

Andersen, K., Azuma, N., Barnola, J., Bigler, M., Biscaye, P., Caillon, N., Chappellaz, J., Clausen, H., Dahl-Jensen, D., Fischer, H., et al., 2004. High-resolution record of Northern Hemisphere climate extending into the last interglacial period. Nature 431 (7005), 147–151.

Andersen, K., Svensson, A., Johnsen, S., Rasmussen, S., Bigler, M., Röthlisberger, R., Ruth, U., Siggaard-Andersen, M., Peder Steffensen, J., Dahl-Jensen, D., et al., 2006. The Greenland ice core chronology 2005, 15–42 ka. Part 1: constructing the time scale. Quaternary Science Reviews 25 (23–24), 3246–3257.

Arnaud, L., Barnola, J., Duval, P., 2000. Physical modeling of the densification of snow/firn 20 and ice in the upper part of polar ice sheets. Physics of Ice Core Records. T. Hondoh. Sapporo.

Basile, I., Petit, J., Touron, S., Grousset, F., Barkov, N., 2001. Volcanic layers in Antarctic(Vostok) ice cores- source identification and atmospheric implications. Journal of Geophysical Research. Atmospheres 106(D23) (31), 915–931.

Blunier, T., Brook, E., 2001. Timing of millennial-scale climate change in Antarctica and Greenland during the last glacial period. Science 291 (5501), 109–112.

Blunier, T., Spahni, R., Barnola, J.-M., Chappellaz, J., Loulergue, L., Schwander, J., 2007. Synchronization of ice core records via atmospheric gases. Climate of the Past 3 (2), 325–330. http://www.clim-past.net/3/325/2007/.

Caillon, N., Severinghaus, J., Barnola, J., Chappellaz, J., Jouzel, J., Parrenin, F., 2001. Estimation of temperature change and of gas age – ice age difference, 108 kyr B.P., at Vostok, Antarctica. Journal of Geophysical Research. D. Atmospheres 106(D23) (31), 893–901.

Caillon, N., Severinghaus, J., Jouzel, J., Barnola, J., Kang, J., Lipenkov, V., 2003. Timing of atmospheric CO_2 and Antarctic temperature changes across termination III. Science 299 (5613), 1728–1731.

Clark, P.U., McCabe, A.M., Mix, A.C., Weaver, A.J., 2004. Rapid rise of sea level 19,000 years ago and its global implications. Science 2304, 1141–1144.

Dreyfus, G.B., Parrenin, F., Lemieux-Dudon, B., Durand, G., Masson-Delmotte, V., Jouzel, J., Barnola, J.-M., Panno, L., Spahni, R., Tisserand, A., Siegenthaler, U., Leuenberger, M., 2007. Anomalous flow below 2700 m in the Dome C ice core detected using $\delta^{18}O$ of atmospheric oxygen measurements. Climate of the Past 3 (2), 341–353. http://www.clim-past.net/3/341/2007/.

Dreyfus Boissier, G., 2008. La composition isotopique de l'air piégé dans la glace: interprétation climatique et outil chronologique. Ph.D. thesis.

Dunbar, N., McIntosh, W., Esser, R., 2008. Physical setting and tephrochronology of the summit Caldera ice record at Mount Moulton, West Antarctica. Bulletin of the Geological Society of America 120 (7–8), 796–812.

Durand, G., Gillet-Chaulet, F., Svensson, A., Gagliardini, O., Kipfstuhl, S., Meyssonnier, J., Parrenin, F., Duval, P., Dahl-Jensen, D., 2007. Change in ice rheology during climate variations – implications for ice flow modelling and dating of the epica dome c core. Climate of the Past 3 (1), 155–167. http://www.clim-past.net/3/155/2007/.

EPICA Community Members, 2004. Eight glacial cycles from an Antarctic ice core. Nature 429, 623–628.

EPICA Community Members, 2006. One-to-one coupling of glacial climate variability in Greenland and Antarctica. Nature 444, 195–198.

Fleitmann, D., Cheng, H., Badertscher, S., Edwards, R., Mudelsee, M., Göktürk, O., Fankhauser, A., Pickering, R., Raible, C., Matter, A., et al., 2009. Timing and climatic impact of Greenland interstadials recorded in stalagmites from northern Turkey. Geophysical Research Letters 36 (19), L19707.

Gilbert, J., Lemarechal, C., 1993. The modules M1QN3 and N1QN3. Program documentation, INRIA.

Goujon, C., Barnola, J., Ritz, C., 2003. Modeling the densification of polar firn including heat diffusion: application to close-off characteristics and gas isotopic fractionation for Antarctica and Greenland sites. Journal of Geophysical Research. Atmospheres 108 (D24), 4792.

Grinsted, A., Dahl-Jensen, D., 2002. A Monte Carlo-tuned model of the flow in the NorthGRIP area. Annals of Glaciology 35 (1), 527–530.

Huber, C., Leuenberger, M., Spahni, R., Flückiger, J., Schwander, J., Stocker, T., Johnsen, S., Landais, A., Jouzel, J., 2006. Isotope calibrated Greenland temperature record over Marine Isotope Stage 3 and its relation to CH_4. Earth and Planetary Science Letters 243 (3–4), 504–519.

Huybrechts, P., 2002. Sea-level changes at the LGM from ice-dynamic reconstructions of the Greenland and Antarctic ice sheets during the glacial cycles. Quaternary Science Reviews 21 (1–3), 203–231.

Huybrechts, P., Rybak, O., Pattyn, F., Ruth, U., Steinhage, D., 2007. Ice thinning, upstream advection, and non-climatic biases for the upper 89% of the EDML ice core from a nested model of the Antarctic ice sheet. Climate of the Past 3 (4), 577–589. http://www.clim-past.net/3/577/2007/.

Johnsen, S., Dahl-Jensen, D., Gundestrup, N., Steffensen, J., Clausen, H., Miller, H., Masson-Delmotte, V., Sveinbjörnsdottir, A., White, J., 2001. Oxygen isotope and palaeotemperature records from six Greenland ice-core stations: camp century, Dye-3, GRIP, GISP2, Renland and NorthGRIP. Journal of Quaternary Science 16 (4), 299–307.

Jouzel, J., Masson-Delmotte, V., Cattani, O., Dreyfus, G., Falourd, S., Hoffmann, G., Minster, B., Nouet, J., Barnola, J., Chappellaz, J., et al., 2007. Orbital and millennial Antarctic climate variability over the past 800,000 years. Science 317 (5839), 793.

Landais, A., Barnola, J., Kawamura, K., Caillon, N., Delmotte, M., Van Ommen, T., Dreyfus, G., Jouzel, J., Masson-Delmotte, V., Minster, B., et al., 2006a. Firn-air δ15N in modern polar sites and glacial–interglacial ice: a model-data mismatch during glacial periods in Antarctica? Quaternary Science Reviews 25 (1–2), 49–62.
Landais, A., Masson-Delmotte, V., Jouzel, J., Raynaud, D., Johnsen, S., Huber, C., Leuenberger, M., Schwander, J., Minster, B., 2006b. The glacial inception as recorded in the NorthGRIP Greenland ice core: timing, structure and associated abrupt temperature changes. Climate Dynamics 26 (2), 273–284.
Lemieux-Dudon, B., Parrenin, F., Blayo, E., 2009. A probabilistic method to construct an optimal ice chronology for ice cores. In: Hondoh, T. (Ed.), Proceedings of the 2nd International Workshop on Physics of Ice Core Records (PICR-2). Institute of Low Temperature Science, Hokkaido University, Sapporo, Japan, in press.
Loulergue, L., Parrenin, F., Blunier, T., Barnola, J.-M., Spahni, R., Schilt, A., Raisbeck, G., Chappellaz, J., 2007. New constraints on the gas age-ice age difference along the epica ice cores, 0–50 kyr. Climate of the Past 3 (3), 527–540. http://www.clim-past.net/3/527/2007/.
Loulergue, L., Schilt, A., Spahni, R., Masson-Delmotte, V., Blunier, T., Lemieux, B., Barnola, J., Raynaud, D., Stocker, T., Chappellaz, J., 2008. Orbital and millennial-scale features of atmospheric CH_4 over the past 800,000 years. Nature 453 (7193), 383–386.
Narcisi, B., Petit, J., Delmonte, B., Basile-Doelsch, I., Maggi, V., 2005. Characteristics and sources of tephra layers in the EPICA-Dome C ice record (East Antarctica): implications for past atmospheric circulation and ice core stratigraphic correlations. Earth and Planetary Science Letters 239 (3–4), 253–265.
Narcisi, B., Petit, J., Tiepolo, M., 2006. A volcanic marker (92 kyr) for dating deep East Antarctic cores. Quaternary Science Reviews 25, 21–22.
Oerter, H., Wilhelms, F., Jung-Rothenhausler, F., Goktas, F., Miller, H., Graf, W., Sommer, S., 2000. Accumulation rates in Dronning Maud land, Antarctica, as revealed by dielectric-profiling measurements of shallow firn cores. Annals of Glaciology 30, 27–34.
Parrenin, F., Barnola, J.-M., Beer, J., Blunier, T., Castellano, E., Chappellaz, J., Dreyfus, G., Fischer, H., Fujita, S., Jouzel, J., Kawamura, K., Lemieux-Dudon, B., Loulergue, L., Masson-Delmotte, V., Narcisi, B., Petit, J.-R., Raisbeck, G., Raynaud, D., Ruth, U., Schwander, J., Severi, M., Spahni, R., Steffensen, J.P., Svensson, A., Udisti, R., Waelbroeck, C., Wolff, E., 2007a. The EDC3 chronology for the EPICA Dome C ice core. Climate of the Past 3 (3), 485–497. http://www.clim-past.net/3/485/2007/.
Parrenin, F., Dreyfus, G., Durand, G., Fujita, S., Gagliardini, O., Gillet, F., Jouzel, J., Kawamura, K., Lhomme, N., Masson-Delmotte, V., Ritz, C., Schwander, J., Shoji, H., Uemura, R., Watanabe, O., Yoshida, N., 2007b. 1-D-ice flow modelling at EPICA dome C and dome Fuji, East Antarctica. Climate of the Past 3 (2), 243–259. http://www.clim-past.net/3/243/2007/.
Parrenin, F., Jouzel, J., Waelbroeck, C., Ritz, C., Barnola, J., 2001. Dating the Vostok ice core by an inverse method. Journal of Geophysical Research. Atmospheres 106(D23) (31), 837–851.
Parrenin, F., Remy, F., Ritz, C., Siegert, M., Jouzel, J., 2004. New modeling of the Vostok ice flow line and implication for the glaciological chronology of the Vostok ice core. Journal of Geophysical Research D20102.
Pattyn, F., 2003. A new three-dimensional higher-order thermomechanical ice sheet model: basic sensitivity, ice stream development, and ice flow across subglacial lakes. Journal of Geophysical Research 108(B8) (2382), 10–1029.
Petit, J., Jouzel, J., Raynaud, D., Barkov, N., Barnola, J., Basile, I., Bender, M., Chappellaz, J., Davis, M., Delaygue, G., et al., 1999. Climate and atmospheric history of the past 420, 000 years from the Vostok ice core, Antarctica. Nature 399 (6735), 429–436.
Pimienta, P., 1987. Etude du comportement mecanique des glaces polycristallines aux faibles contraintes. Ph.D. thesis, These de 1'Universite Joseph Fourier-Grenoble I.
Raisbeck, G.M., Yiou, F., Jouzel, J., Stocker, T.F., 2007. Direct north-south synchronization of abrupt climate change record in ice cores using beryllium 10. Climate of the Past 3 (3), 541–547. http://www.clim-past.net/3/541/2007/.
Rasmussen, S., Andersen, K., Svensson, A., Steffensen, J., Vinther, B., Clausen, H., Siggaard-Andersen, M., Johnsen, S., Larsen, L., Dahl-Jensen, D., et al., 2006. A new Greenland ice core chronology for the last glacial termination. J. Geophys. Res 111.
Rasmussen, S., Seierstad, I., Andersen, K., Bigler, M., Dahl-Jensen, D., Johnsen, S., 2008. Synchronization of the NGRIP, GRIP, and GISP2 ice cores across MIS 2 and palaeoclimatic implications. Quaternary Science Reviews 27 (1–2), 18–28.
Ritz, C., Rommelaere, V., Dumas, C., 2001. Modeling the evolution of Antarctic ice sheet over the last 420, 000 years- Implications for altitude changes in the Vostok region. Journal of Geophysical Research. Atmospheres 106(D23) (31), 943–964.
Rotschky, G., Eisen, O., Wilhelms, F., Nixdorf, U., Oerter, H., 2004. Spatial distribution of surface mass balance on Amundsenisen plateau, Antarctica, derived from ice-penetrating radar studies. Annals of Glaciology 39, 265.
Ruth, U., Barnola, J.-M., Beer, J., Bigler, M., Blunier, T., Castellano, E., Fischer, H., Fundel, F., Huybrechts, P., Kaufmann, P., Kipfstuhl, S., Lambrecht, A., Morganti, A., Oerter, H., Parrenin, F., Rybak, O., Severi, M., Udisti, R., Wilhelms, F., Wolff, E., 2007. EDML1: a chronology for the EPICA deep ice core from Dronning Maud land, Antarctica, over the last 150,000 years. Climate of the Past 3 (3), 475–484. http://www.clim-past.net/3/475/2007/.
Severi, M., Becagli, S., Castellano, E., Morganti, A., Traversi, R., Udisti, R., Ruth, U., Fischer, H., Huybrechts, P., Wolff, E., Parrenin, F., Kaufmann, P., Lambert, F., Steffensen, J.P., 2007. Synchronisation of the EDML and EDC ice cores for the last 52 kyr by volcanic signature matching. Climate of the Past 3 (3), 367–374. http://www.clim-past.net/3/367/2007/.
Severinghaus, J., Sowers, T., Brook, E., Alley, R., Bender, M., 1998. Timing of abrupt climate change at the end of the Younger Dryas interval from thermally fractionated gases in polar ice. Nature 391, 141–146.
Stocker, T., 1998. Climate change: the seesaw effect. Science 282 (5386), 61.
Svensson, A., Andersen, K., Bigler, M., Clausen, H., Dahl-Jensen, D., Davies, S., Johnsen, S., Muscheler, R., Rasmussen, S., Röthlisberger, R., et al., 2006. The Greenland ice core chronology 2005, 15–42 ka. Part 2: comparison to other records. Quaternary Science Reviews 25 (23–24), 3258–3267.
Svensson, A., Andersen, K.K., Bigler, M., Clausen, H.B., Dahl-Jensen, D., Davies, S.M., Johnsen, S.J., Muscheler, R., Parrenin, F., Rasmussen, S.O., Röthlisberger, R., Seierstad, I., Steffensen, J.P., Vinther, B.M., 2008. A 60,000 year Greenland Stratigraphic ice core chronology. Climate of the Past 4 (1), 47–57. http://www.clim-past.net/4/47/2008/.
Traufetter, F., Oerter, H., Fischer, H., Weller, R., Miller, H., 2004. Spatio-temporal variability in volcanic sulphate deposition over the past 2 kyr in snow pits and firn cores from Amundsenisen, Antarctica. Journal of Glaciology 50 (168), 137–146.
Udisti, R., Becagli, S., Castellano, E., Delmonte, B., Jouzel, J., Petit, J., Schwander, J., Stenni, B., Wolff, E., 2004. Stratigraphic correlations between the European project for ice coring in Antarctica (EPICA) Dome C and Vostok ice cores showing the relative variations of snow accumulation over the past 45 kyr. Journal Geophysical Research. Atmospheres 109 (D08), 101.
Yiou, F., Raisbeck, G., Baumgartner, S., Beer, J., Hammer, C., Johnsen, S., Jouzel, J., Kubik, P., Lestringuez, J., Stievenard, M., et al., 1997. Beryllium 10 in the Greenland ice core project ice core at summit, Greenland. Journal of Geophysical Research 102 (C 12), 26783–26794.